J|A|C|S
ARTICLES

Published on Web 09/16/2009

One-Pot Room-Temperature Synthesis of Single-Crystalline Gold Nanocorolla in Water

Tetsuro Soejima and Nobuo Kimizuka*

Department of Chemistry and Biochemistry, Graduate School of Engineering, Kyushu University and JST, CREST, 744 Moto-oka, Nishi-ku, Fukuoka 819-0395, Japan

Received June 15, 2009; E-mail: n-kimi@mail.cstm.kyushu-u.ac.jp

Abstract: A room-temperature nanocarving strategy is developed for the fabrication of complex gold nanoplates having corolla- and propeller-like architectures. It is based on the simultaneous growth and etching of gold nanoplates in aqueous solution, which occur in the course of photoreduction of $Au(OH)_4^-$ ions. The presence of bromide ion, poly(vinylpyrrolidone) (PVP), and molecular oxygen is indispensable, where bromide ions play multiple roles. First, they promote formation of nanoplate structures by forming adlayers on the fcc(111) surface. Second, they facilitate oxidative dissolution of gold nanocrystals by converting the oxidized Au(I) species to soluble $AuBr_2^-$ ions, which lead to the formation of ultrathin nanocrevasses. PVP also stabilizes the nucleation of gold nanoplates. Although the overall reactions proceed in one-pot, the crystal growth and etching show interplay and occur with different kinetics due to changes in the concentration of $Au(OH)_4^-$ and other species with time. Corolla- or propeller-like gold nanoplates formed under these conditions are single-crystalline, as indicated by selected area electron diffraction patterns and the observation of moiré fringes. The morphology of corolla- or propeller-like gold nanoplates is controllable depending on the concentration of bromide ion and PVP in the aqueous mixture. On the basis of these results, a preliminary mechanism is proposed which involves the concurrent crystal growth and oxidative etching on the surface of nanocrystals.

Introduction

Gold nanocrystals have attracted considerable attention because of their intriguing optical and catalytic properties, which are distinct from those in the bulk state. For example, the surface plasmon resonance properties, which originate from the collective oscillation of their conduction electrons in response to optical excitation, strongly depend on the size,[1] surface modification,[2] and aggregate morphology.[3] Although gold has been considered to be chemically inert for a long time, gold nanocrystals with diameters of less than 10 nm become active catalysts when they are dispersed on metal oxides.[4] Thus, physicochemical properties of gold nanocrystals are controllable depending on their surface and interfacial structures (i.e., the surface area per unit volume, crystallographic facets displayed on surfaces, and their environment). Consequently, the development of synthetic methodologies for nonspherical gold nanocrystals has been an important issue of fundamental research, which is stimulated by the growth of numerous applications such as new optical devices,[5] chemical sensing,[6] and catalysis.[7]

To date, synthetic routes for anisotropic nanostructures such as rods,[8] wires,[9] and plates[10] have been accumulated. Synthetic approaches for these common nanocrystals usually make use of templates where crystal growth is regulated by interfaces such provided by surfactant micelles or porous alumina membranes.[11] The anisotropic growth of nanocrystals is also assisted by polymer stabilizers such as poly(vinylpyrrolidone) (PVP), which influences the growth rate of different crystalline facets by interacting through adsorption.[12]

With all the progress in synthetic methodologies for these typical nonspherical nanocrystals, however, development of synthetic approaches for those with higher-order complexities (i.e., branched nanocrystals,[13] star-shaped nanocrystals,[14] holey nanocrystals,[15] and tadpoles)[16] is still in its infancy. One of the rational approaches toward this issue is to etch preformed nanocrystals into complex nanostructures. For example, porous

(1) (a) Kreibig, U.; Genzel, L. *Surf. Sci.* **1985**, *156*, 678. (b) Murphy, C. J.; Jana, N. R. *Adv. Mater.* **2002**, *14*, 80.
(2) Caruso, R. A.; Antonietti, M. *Chem. Mater.* **2001**, *13*, 3272.
(3) Elghanian, R.; Storhoff, J. J.; Mucic, R. C.; Letsinger, R. L.; Mirkin, C. A. *Science* **1997**, *277*, 1078.
(4) Ishida, T.; Haruta, M. *Angew. Chem., Int. Ed.* **2007**, *46*, 7154.
(5) Stewart, M. E.; Anderton, C. R.; Thompson, L. B.; Maria, J.; Gray, S. K.; Rogers, J. A.; Nuzzo, R. G. *Chem. Rev.* **2008**, *108*, 494.
(6) Murphy, C. J.; Sau, T. K.; Gole, A. M.; Orendorff, C. J.; Gao, J.; Gou, L.; Hunyadi, S. E.; Li, T. *J. Phys. Chem. B* **2005**, *109*, 13857.
(7) Hashmi, A. S. K.; Hutchings, G. J. *Angew. Chem., Int. Ed.* **2006**, *45*, 7896.
(8) (a) Murphy, C. J.; Gole, A. M.; Hunyadi, S. E.; Orendorff, C. J. *Inorg. Chem.* **2006**, *45*, 7544. (b) Hurst, S. J.; Payne, E. K.; Qin, L.; Mirkin, C. A. *Angew. Chem., Int. Ed.* **2006**, *45*, 2672.
(9) Xia, Y.; Yang, P.; Sun, Y.; Wu, Y.; Mayers, B.; Gates, B.; Yin, Y.; Kim, F.; Yan, H. *Adv. Mater.* **2003**, *15*, 353.
(10) (a) Millstone, J. E.; Park, S.; Shuford, K. L.; Qin, L.; Schatz, G. C.; Mirkin, C. A. *J. Am. Chem. Soc.* **2005**, *127*, 5312. (b) Xue, C.; Métraux, G. S.; Millstone, J. E.; Mirkin, C. A. *J. Am. Chem. Soc.* **2008**, *130*, 8337.
(11) Pérez-Juste, J.; Pastoriza-Santos, I.; Liz-Marzán, L. M.; Mulvaney, P. *Coord. Chem. Rev.* **2005**, *249*, 1870.
(12) Xiong, Y.; Washio, I.; Chen, J.; Cai, H.; Li, Z.-Y.; Xia, Y. *Langmuir* **2006**, *22*, 8563.
(13) Wu, H.-L.; Chen, C.-H.; Huang, M. H. *Chem. Mater.* **2009**, *21*, 110.
(14) Nehl, C. L.; Liao, H.; Hafner, J. H. *Nano Lett.* **2006**, *6*, 683.

gold nanowires[17] and films[18] are obtained by dissolving silver components from preformed Ag−Au alloy nanowires and films, respectively. Stucky et al. reported that single-crystalline gold nanorods were shortened in the presence of cetyltrimethylammonium bromide and molecular oxygen, indicating that the nanorods underwent oxidative dissolution selectively at termini.[19] In these conventional approaches, etching procedures are separately applied to metal nanocrystals which have been synthesized in advance.

An alternative and more straightforward strategy is to concurrently perform both of the growth and etching processes in one step, by taking advantage of different reactivities revealed by each nanocrystal facet. However, it is generally difficult to shape nanocrystals by this simultaneous build-and-etch approach, since the crystal growth and dissolution processes usually occur for different nanocrystals coexisting in the reaction mixture. For example, Xia et al. reported the growth of silver truncated nanocubes at the expense of twinned single-crystal particles.[20] Thus, sculpting nanocrystals by the concurrent build-and-etch approach remains a green field. To work on this issue, we selected a two-dimensional gold nanoplate as a basic nanostructure, since etching-directed morphological control of gold nanoplates has been largely unexplored. Metal nanoplates also show unique optical properties that are distinct from isotropic nanoparticles or one-dimensional nanorods. For example, they display two-photon-induced photoluminescence (PL) properties that are much stronger than those of nanorods.[21] Their catalytic activity in hydrogen generation was shown to be higher than those reported for nanoparticles and nanorods.[22] These features make nanoplates attractive candidates for a number of applications such as optical biosensing,[23] substrates for surface-enhanced Raman scattering,[24] and refractive index sensors.[25] In addition, one of the salient features in nanoplates lies in the presence of their sharp edges, which gave high local electric field gradients under photoillumination.[26] Therefore, if edges can be introduced inside nanoplates as higher energy crevasses, they may add unique physicochemical properties to nanoplates.

Recently, Guo et al. reported that the reduction of $HAuCl_4$ by aniline in aqueous HCl gave irregularly layered gold nanoplates, where the rate of reduction was slowed because of oxidative etching of gold atoms by Cl^- ions.[27] However, in their synthetic system, the causal relationship between the oxidative etching and morphology remains unclear. Here, we report one-step nanocarving of gold nanoplates through simultaneous crystal growth and oxidative etching processes. This nanocarving approach gives rise to unprecedented, corolla- or propeller-like single-crystalline gold nanoarchitectures in water at ambient temperature.

Scheme 1. Schematic Illustration of the Synthesis of Gold Nanoplates Which Are Synchronized with Crystal Growth and Etching Processes

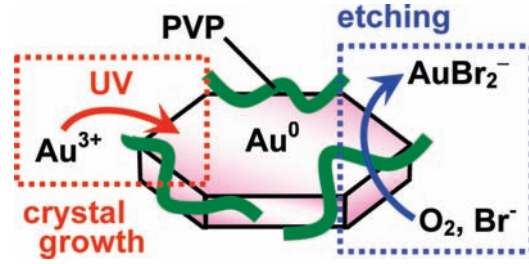

Experimental Section

$HAuCl_4 \cdot 4H_2O$ (99%) was supplied by Kanto Chemical Co. Ltd. PVP and NaBr (>99%) were obtained from Kishida Chemical Co. Ltd. The stock solution of aqueous $AuCl_4^-$ solution was prepared by dissolving 1 g of $HAuCl_4 \cdot 4H_2O$ in 100 mL of water. The pH of a 24.3 mM aqueous $AuCl_4^-$ solution was adjusted to 10.0 by the addition of aqueous 1 M NaOH. The yellow solution turned colorless, which reflected the ligand exchange from $AuCl_4^-$ to $Au(OH)_4^-$.[28] To this solution (1 mL), 0.2 mL of 100 mM aqueous NaBr solution was added. When powdery PVP (0.3 g) was further added to this colorless solution, the color of the solution turned yellow. The yellow solution in a sample tube was then irradiated with a high-pressure mercury lamp ($\lambda_{300-400}$ = 16 mW/cm^2, UI-501C, Ushio) at 20 °C.

Results and Discussion

Scheme 1 illustrates the one-pot build-and-etch strategy developed in this study. This reaction system is composed of two processes that occur concurrently. One is the growth of two-dimensional gold(0) nanoplates that occur by photoreduction of $Au(OH)_4^-$ complexes.[15] The other is oxidative etching of gold nanoplates by dissolved molecular oxygen. In these processes, bromide ions play multiple tasks. First, they form stable adlayers on gold surfaces[30] and promote the growth of two-dimensional nanoplates. Second, they facilitate the oxidative etching of gold nanocrystals, by converting the oxidized Au(I) species to $AuBr_2^-$ ions soluble in water.[19] Thus, both crystal growth and etching occur simultaneously on the same or different facets of each nanocrystal. PVP was employed as surface stabilizer for nanoplates.[12]

Upon photoillumination of the aqueous mixture containing $Au(OH)_4^-$, PVP, and NaBr, the yellow color changed to purple-black, indicating progress of the photoreduction of $Au(OH)_4^-$ ions to gold nanocrystals (Figure 1a). Transmission electron microscopy (TEM) images of gold nanocrystals formed at varied NaBr concentrations are shown in Figure 1b−e. In the absence of NaBr ($[Br^-]$ = 0 M), only winding nanowires were found (Figure 1b). In contrast, flowerlike nanoplates with size up to 300 nm were abundantly observed in the presence of bromide ions (Figures 1c and S1a in the Supporting Information, [NaBr] = 16.7 mM). Apparently, bromide ions are required to form 2D nanoplates. This is reasonable since bromide ions show

(15) Soejima, T.; Morikawa, M-a.; Kimizuka, N. *Small* [Online Early Access]. DOI: 10.1002/smll.200900348. Published Online: May 21, **2009**.
(16) Soejima, T.; Hasegawa, T.; Morikawa, M-a.; Kimizuka, N. *Chem. Lett.* **2009**, *38*, 688.
(17) Ji, C.; Searson, P. C. *J. Phys. Chem. B* **2003**, *107*, 4494.
(18) Li, R.; Sieradzki, K. *Phys. Rev. Lett.* **1992**, *68*, 1168.
(19) Tsung, C.-K.; Kou, X.; Shi, Q.; Zhang, J.; Yeung, M. H.; Wang, J.; Stucky, G. D. *J. Am. Chem. Soc.* **2006**, *128*, 5352.
(20) Wiley, B.; Herricks, T.; Sun, Y.; Xia, Y. *Nano Lett.* **2004**, *4*, 1733.
(21) Imura, K.; Nagahara, T.; Okamoto, H. *Appl. Phys. Lett.* **2006**, *88*, 023104.
(22) Bi, Y.; Lu, G. *Mater. Lett.* **2008**, *62*, 2696.
(23) Chen, Y.; Munechika, K.; Ginger, D. S. *Nano Lett.* **2007**, *7*, 690.
(24) Zou, X.; Dong, S. *J. Phys. Chem. B* **2006**, *110*, 21545.
(25) Rashid, M. H.; Bhattacharjee, R. R.; Mandal, T. K. *J. Phys. Chem. C* **2007**, *111*, 9684.
(26) Grzelczak, M.; Pérez-Juste, J.; Mulvaney, P.; Liz-Marzán, L. M. *Chem. Soc. Rev.* **2008**, *37*, 1783.
(27) Guo, Z.; Zhang, Y.; Xu, A.; Wang, M.; Huang, L.; Xu, K.; Gu, N. *J. Phys. Chem. C* **2008**, *112*, 12638.
(28) (a) Goia, D. V.; Matijević, E. *Colloids Surf., A* **1999**, *146*, 139. (b) Ivanova, S.; Petit, C.; Pitchon, V. *Appl. Catal., A* **2004**, *267*, 191.
(29) Ha, T. H.; Koo, H.-J.; Chung, B. H. *J. Phys. Chem. C* **2007**, *111*, 1123.
(30) Magnussen, O. M. *Chem. Rev.* **2002**, *102*, 679.

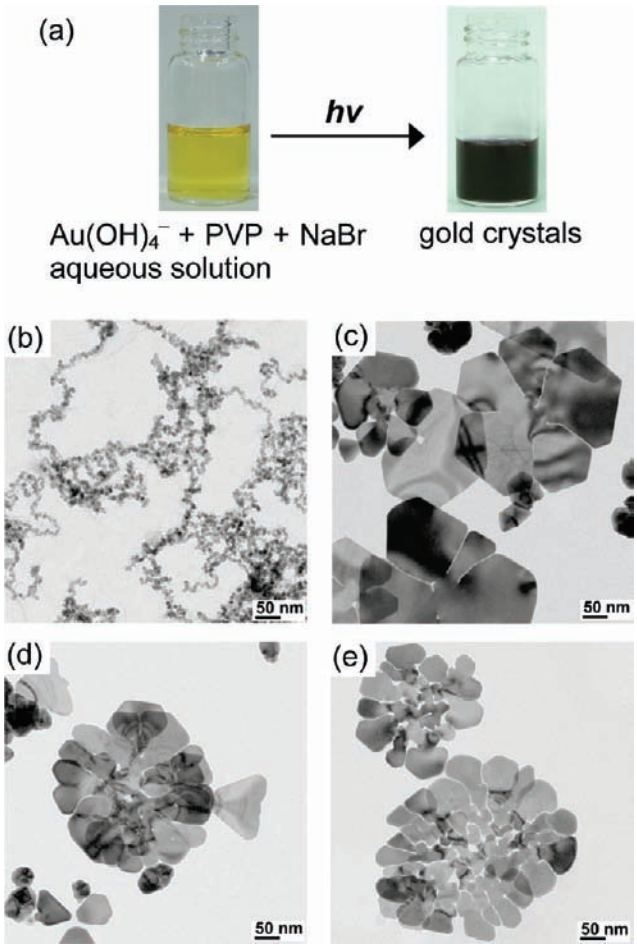

Figure 1. (a) Pictures of a sample before (left) and after (right) photoirradiation. TEM images of the flowerlike gold nanoplates obtained at varied NaBr concentration: (b) 0 M, (c) 16.7 mM, (d) 50.0 mM, (e) 167 mM. $[Au(OH)_4^-] = 18.0$ mM. [PVP] = 0.25 g/mL. Irradiation time = 2 h.

propensity to strongly bind to gold(111) surfaces and form stable adlayers.[30] It inhibits the growth of {111} facets and results in the crystal growth to lateral {110} direction.[26] The whole flower-shaped nanocrystals and the branched parts are hereafter referred to as "corolla" and "petals", respectively, by structural analogy with botanical flowers (Figure S2 in the Supporting Information). Interestingly, the crevasses formed between each petal are surprisingly narrow as 1 nm (Figure S1b in the Supporting Information); the distance corresponds only to ca. five gold atoms. Upon further increasing the NaBr concentration to 50.0 mM (Figure 1d) and 167 mM (Figure 1e), the number of crevasses remarkably increased and highly complex nanoarchitectures were obtained. The observed formation of crevasses is ascribed to oxidative etching of gold nanocrystals mediated by bromide ions,[19,20] which became significant when the concentration of NaBr exceeded twice that of gold ions (Figure 1, panel c vs d, $[Au(OH)_4^-] = 18$ mM). As will be discussed later, this would be related to the etching mechanism, where gold atoms are dissolved as anionic bromide complexes such as $AuBr_2^-$.[19] Thus, bromide ions are involved in both of the growth and etching processes and concentration of bromide ions is a decisive factor that determines the morphology of gold nanocrystals.

Vis−near-infrared (vis−NIR) spectra obtained for these nanocrystals are shown in Figure 2. The winding nanowires (Figure 1b) showed a broad peak with a maximum at ~600 nm

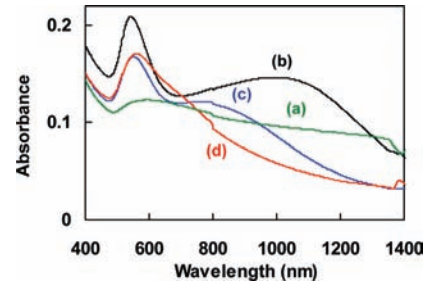

Figure 2. Vis−NIR absorption spectra of the flowerlike gold nanoplates aqueous dispersions obtained at varied NaBr concentration: (a) 0 M, (b) 16.7 mM, (c) 50.0 mM, (d) 167 mM. $[Au(OH)_4^-] = 18.0$ mM. [PVP] = 0.25 g/mL. Irradiation time = 2 h.

(Figure 2a), which is similar to the plasmon absorption reported for gold nanowires.[15] On the other hand, corollaceous gold nanoplates showed an intense absorption peak around 1100 nm (Figure 2b, [NaBr] = 16.7 mM), which is assignable to the dipole plasmon resonance absorption for nanoplates.[31] A peak coexisting at 533 nm is ascribed to that of spherical nanocrystals that are formed concomitantly (Figure S3a,d,e in the Supporting Information). As the concentration of bromide ion is increased, the dipole resonance absorption peak showed blue-shifts with gradual decrease in the intensity (Figure 2b−d). The observed disappearance of dipole plasmon resonance absorption at the near-infrared region reflects the decrease in the (111) surface area, which occurred as a consequence of developed crevasse formation. That is, the extended delocalization of the in-plane electrons is restricted by the crevasses. This observation is consistent with the dependence of plasmon resonance on the edge length reported for gold nanoprisms.[31]

Figure 3 shows TEM images and a selected area electron diffraction (SAED) pattern of a propeller-like gold nanoplate, which was formed together with the corollaceous nanoplates. The electron diffraction patterns observed for these gold nanoplates showed a series of diffraction spots with a sixfold rotational symmetry, which could be indexed to {220} planes of face-centered cubic (fcc) gold and to the formally forbidden 1/3{422} reflections (Figure 3b). A high-resolution TEM (HRTEM) image of the gold nanoplates showed fringes with a spacing of 0.25 nm, which corresponds to the 1/3{422} reflection (Figure 3c). The fcc forbidden 1/3{422} reflections occur because of the presence of (111) stacking fault(s) lying parallel to the (111) surface and extending across the entire planar particle.[32a] These observations indicate that the surface of gold nanoplates is indexed as flat (111) planes of fcc lattice, with atomically flat structure.[32]

Figure 3d shows a TEM lattice image of a nanoplate around a crevasse. Both crystal edges facing the crevasse show completely identical orientation of the crystal lattice, indicating that the crevasse was formed by etching a single crystalline nanosheet. Very interestingly, the growth of nanocrystals occurred even at the edge of crevasses, as shown by the formation of three-dimensional nanopropeller structures (Figure 4a). Distinct moiré fringes were observed at the overlapped portions of these nanopropellers (Figure 4b−d), which corroborate the observed SAED pattern and prove that they consist of a single crystal with homogeneous thickness. The thickness

(31) Millstone, J. E.; Métraux, G. S.; Mirkin, C. A. *Adv. Funct. Mater.* **2006**, *16*, 1209.
(32) (a) Germain, V.; Li, J.; Ingert, D.; Wang, Z. L.; Pileni, M. P. *J. Phys. Chem. B* **2003**, *107*, 8717. (b) Jin, R.; Cao, Y.; Mirkin, C. A.; Kelly, K. L.; Schatz, G. C.; Zheng, J. G. *Science* **2001**, *294*, 1901.

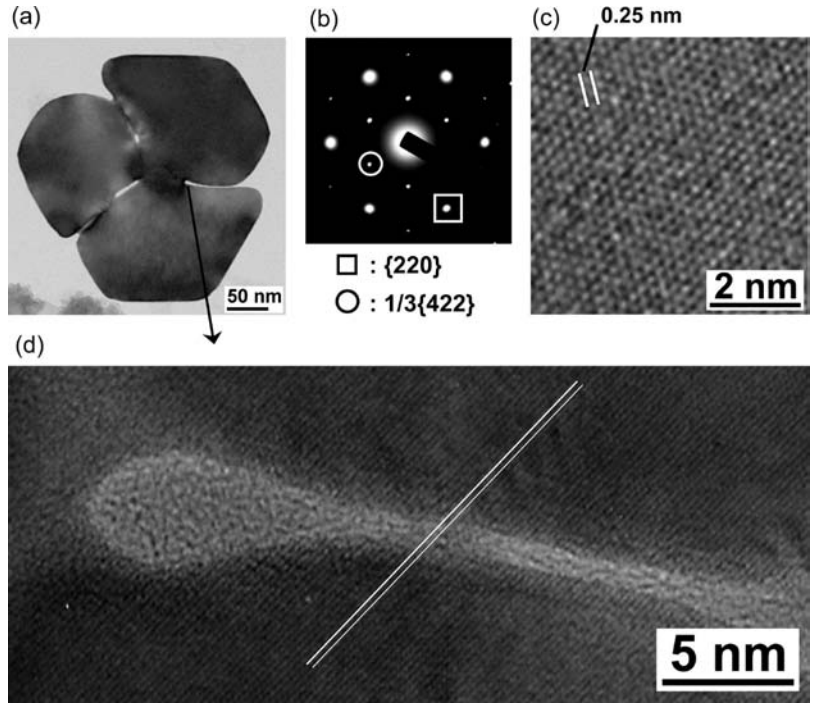

Figure 3. Transmission electron micrograph of gold nanopropeller (a), SAED pattern (b), HRTEM image of a lattice structure observed for the (111) surface of gold nanoplate (c), and lattice structure of gold nanoplates around a crevasse (d). Nanoplates were obtained under the condition of $[Au(OH)_4^-]$ = 18.0 mM. [NaBr] = 16.7 mM. [PVP] = 0.25 g/mL. Irradiation time = 6 h. The fraction of nanopropeller in nanocorolla was ca. 6%.

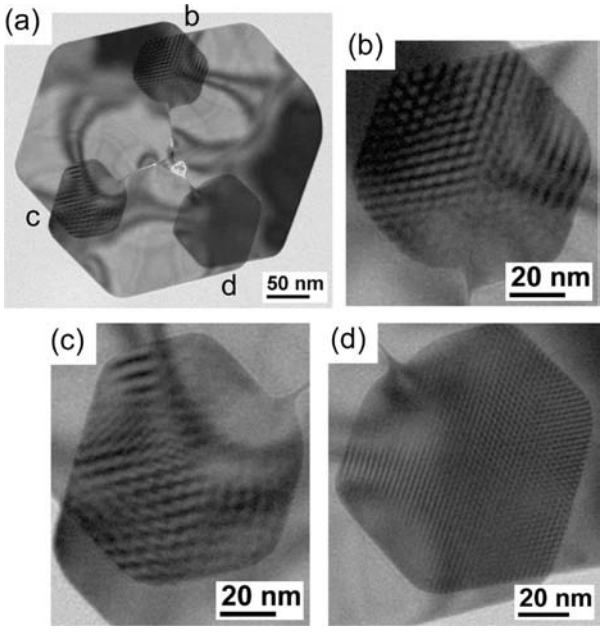

Figure 4. TEM images of propeller-like gold nanoplates. Moiré fringes are clearly seen at the overlapped portions (b, c, d), indicating that the propeller nanoplate consists of a single crystal. Nanoplates were synthesized under these conditions. $[Au(OH)_4^-]$ = 18.0 mM. [NaBr] = 16.7 mM. [PVP] = 0.25 g/mL. Irradiation time = 6 h.

of each nanoplate would be sufficiently thin so as to give moiré fringes, in the order of 10−20 nm as estimated from the SEM picture shown in Figure S3c in the Supporting Information. The formation of these single-crystalline 3D nanopropellers indicates that the overlapped portion of propeller blade tips has grown after the oxidative etching of nanoplates, providing conclusive evidence that crystal growth and etching processes show interplay and occurred in each nanocrystal concurrently.

X-ray photoelectron spectroscopy (XPS) of corollaceous nanocrystals is shown in Figure S4 in the Supporting Information. An intense peak at 84.0 eV is assigned to the emission from $4f_{7/2}$ electron of gold(0), consistent with the formation of gold nanoplates (upper left in Figure S4b in the Supporting Information). Sharp peaks are observed at the binding energies of 67.8 and 68.6 eV, which are assignable to emissions from $3d_{5/2}$ and $3d_{3/2}$ electrons of bromide ions, respectively (lower left in Figure S4b in the Supporting Information).[33] It supports the presence of bromide adlayers on the gold (111) plane,[29,30] together with the negative ζ potential observed for aqueous dispersion of nanoplates (−30.4 mV at pH 6).[34] On the other hand, a peak is observed at the binding energy of 399.9 eV (lower right in Figure S4 in the Supporting Information), which is assignable to emissions from N1s electrons. It originates from PVP molecules adsorbed on the surface of corollaceous nanoplates. PVP is known to interact with the gold (111) plane,[35] and the presence of adsorbed PVP was confirmed by TEM, where the PVP polymer layer was observed as pale dark contrasts present on the periphery of nanoplates (Figure S5 in the Supporting Information). Figure S6 in the Supporting Information shows TEM images and vis−NIR spectra of gold nanoplates formed under varied PVP concentrations. Developed nanoplates are formed at higher PVP concentration, indicating that PVP also enhances the growth rate along the {110} direction.

To confirm the contribution of molecular oxygen in the oxidative etching process and to elucidate the mechanism, photoirradiation was conducted for deaerated aqueous solutions containing $Au(OH)_4^-$, NaBr, and PVP. Figure S7a,b in the

(33) Hubert, F.; Testard, F.; Spalla, O. *Langmuir* **2008**, *24*, 9219.
(34) van der Zande, B. M. I.; Dhont, J. K. G.; Böhmer, M. R.; Philipse, A. P. *Langmuir* **2000**, *16*, 459.
(35) Kim, F.; Connor, S.; Song, H.; Kuykendall, T.; Yang, P. *Angew. Chem., Int. Ed.* **2004**, *43*, 3673.

Supporting Information compares TEM images of gold nanoplates prepared for aerated and deaerated solutions, respectively. When the solution was deaerated by bubbling argon, gold nanoplates with triangle or hexagonal structures were formed (Figure S7b in the Supporting Information). Although some nanoplates show depressions on the vertexes, these structures are distinct from highly creviced nanoplate structures obtained in the aerated solutions (Figures 1c and S7a in the Supporting Information). Apparently, the formation of nanocrevasses is suppressed in deaerated solutions, indicating that etching reaction requires the presence of oxygen. These structural differences are also reflected in their vis−NIR spectra (Figure S7c in the Supporting Information). The intense, broad absorption intensity around 1000 nm is observed for the gold nanoplates synthesized in the argon-bubbled solution, whereas such an NIR component disappeared upon oxidative etching in the aerated solution.

Oxygen molecules possess high electrochemical potential (E_0 = +1.229 V vs SHE), which is sufficient to oxidize Au^0 to Au^+ or Au^{3+} ions, as shown below.[36]

$$O_2 + 4H^+ + 4e^- \rightarrow 2H_2O \quad E_0 = +1.229 \text{ V vs SHE} \tag{1}$$

$$Au + 2Br^- \rightarrow AuBr_2^- + e^- \quad E_0 = +0.959 \text{ V vs SHE} \tag{2}$$

$$Au + 4Br^- \rightarrow AuBr_4^- + 3e^- \quad E_0 = +0.854 \text{ V vs SHE} \tag{3}$$

In the presence of bromide anions, gold nanocrystals will be oxidatively etched as colorless $AuBr_2^-$ ions[19] or yellow $AuBr_4^-$ ions.[37] Although spectroscopic detection of these ions (absorption peaks; $AuBr_2^-$, 257 nm,[38] $AuBr_4^-$, 255, 380, and 455 nm[39]) is hampered by the overwhelming plasmon absorption band of photogenerated gold nanoplates, formation of these anionic bromide complexes is consistent with the creviced nanoplates formed in aerated solutions (Figures 1c, 3a, and S7a in the Supporting Information).

Figure S8 in the Supporting Information shows TEM images of gold nanoplates obtained at different photoirradiation periods. Small gold nanoparticles and nanoplates are formed after photoirradiating the solution for 1 h (Figures 5a and S8a in the Supporting Information). It is seen that some nanoplates already have pits on vertexes and on edges. This is reasonable since oxidative etching and dissolution would occur preferentially at edges of high surface energy (i.e., at atomic steps on the side and vertexes of gold nanoplates). Typical morphological changes of gold nanocrystals and a plausible oxidative etching model are shown in Figure 5a−c. In Figure S8 in the Supporting Information (a→e), the gold nanoplates grow with time and the average size of nanoplates is increased upon photoirradiation. Nanoplates with irregular structures are also found in these pictures, indicating that they are grown from the pitted nanoplates. After ca. 6 h of photoillumination, on the other hand, formation of flowerlike gold nanoplates became conspicuous (Figure S8f in the Supporting Information). When photoillumination was further continued to a total period of ca. 12 h, the flowerlike structures are finally cut in petal species (Figure S8g in the Supporting Information), probably by running each nanocrevasse through to the other crevasses. It appears that the growth of gold nanoplates is dominant in the initial stage, whereas it became slower upon the consumption of $Au(OH)_4^-$ ions in the bulk solution. Consequently, it is taken over by the oxidative etching of sharp crevasses as shown in Figure S8f in the Supporting Information. The number of crevasses (i.e., high surface energy area grown from pits on the surface) is seemingly rather limited under low bromide concentrations. This is probably because the oxidative dissolution preferentially occurs at the existing high energy surfaces. These observations are consistent with the dependence of vis−NIR spectra on the photoirradiation period (Figure S9 in the Supporting Information).

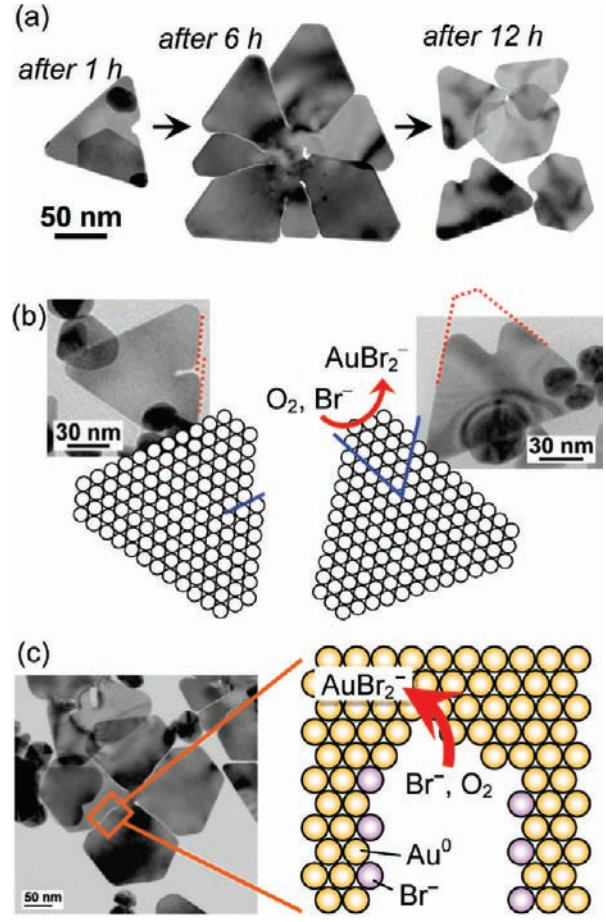

Figure 5. (a) Representative TEM images of the flowerlike gold nanoplates obtained after different photoirradiation times. (b) Edge- or vertex-eroded nanoplates formed after 1 h of photoirradiation and overhead illustration of (111) facet. (c) Schematic illustration of a crevasse formation by preferential oxidative etching of high energy surfaces at the growth front of nanocrevasse. Adlayer of bromide ions on fcc(111) plane is omitted for clarity. $[Au(OH)_4^-]$ = 18.0 mM. [NaBr] = 16.7 mM. [PVP] = 0.25 g/mL.

Surface energies associated with gold crystallographic facets usually increase in the order $\gamma\{111\} < \gamma\{100\} < \gamma\{110\}$,[40] and thus the close-packed {111} surfaces show higher stability compared to the edge surfaces (i.e., Au(110) faces). The observed formation of nanocrevasses shown in Figures 1c−e,

(36) *CRC Handbook of Chemistry and Physics*, 76th ed.; Lide, D. R., Ed.; CRC Press: Boca Raton, FL, 1995.
(37) Dasog, M.; Scott, W. J. *Langmuir* **2007**, *23*, 3381.
(38) Sevas, M. M.; Mason, W. R. *Inorg. Chem.* **1987**, *26*, 301.
(39) Usher, A.; McPhail, D. C.; Brugger, J. *Geochim. Cosmochim. Acta* **2009**, *73*, 3359.
(40) Wang, Z. L. *J. Phys. Chem. B* **2000**, *104*, 1153.

3d, and 5a clearly indicates that oxidative etching occurs preferentially at higher energy edge sites, more specifically, at atomic step edges on Au(110) faces or vertexes of nanoplates. This is reasonable, since oxidative etching of gold requires adsorption of molecular oxygen, which is expedited by the larger coordination number of the edge gold atoms. The higher reactivity of step edges and kink sites is also supported by theoretical considerations.[41,42] Partial electron transfer from the edge surface to the LUMO (π^*) of O_2 would occur, possibly providing superoxo-like intermediates[43,44] as exemplified below.

$$Au^0(\text{edge}) \cdot 2Br^- + O_2 \rightarrow [Au^{\delta+}(\text{edge}) \cdot 2Br^- \cdots O_2^{\delta-}] \quad (4)$$

$$[Au^{\delta+}(\text{edge}) \cdot 2Br^- \cdots O_2^{\delta-}] \rightarrow AuBr_2^- + O_2^- \quad (5)$$

It is generally accepted that gold atoms at surface defect sites such as step edges or kink sites are weakened in their interaction with bulk gold, which can lead to enhanced mobility.[42] Therefore, it does not come as a surprise that the growth front of nanocrevasses has higher reactivity toward oxidative etching. On the other hand, the edge walls of crevasses tend to become smooth to keep a low energy state. As a result, selective etching would have occurred to form nanocrevasses while maintaining the sharp width of ca. 5 nm. It is plausible that these edge walls are also stabilized by the adsorbed bromide ions and PVP. As described herein, the number of nanocrevasses and direction of etching with respect to the outer rim of nanoplates vary depending on the reaction condition (for example, concentrations of bromide ions, oxygen, and PVP). Therefore, the overall morphological transformation is kinetically determined by the dynamic interplays between diffusion, adsorption, photoreduction, complexation, and dissolution processes occurring at the nanointerface.

In conclusion, a one-pot build-and-etch strategy for the fabrication of complex metal nanoarchitecture is developed. This nanocarving technique is based on the concurrent photoreduction and oxidative dissolution processes, and it leads to the formation of unique single-crystalline nanostructures such as corolla- or propeller-like gold nanoplates. Bromide ions exert bimodal effects (i.e., the inhibition of {111} facets by formation of adlayers on the fcc(111) surfaces and the promotion of oxidative dissolution processes). It is noteworthy that surprisingly narrow crevasses with a narrow gap as small as 1 nm are obtained, and the number or density of crevasses were controllable depending on the concentration of bromide ions. Although the overall reactions proceed in one-pot, the crystal growth and oxidative dissolution show dynamic interplay and occur with different kinetics at nanointerfaces which are affected by the changes in concentration of $Au(OH)_4^-$ and the other species over time. These features lead to the emergence of complex single-crystalline nanoarchitectures. The simultaneous build-and-etch approach developed in this study is simple and may lead to a rich variety of complex single-crystalline nanocrystals.[45] Together with holey gold nanowires synthesized under far-from-equilibrium conditions,[15] we envisage that complex metal nanoarchitecture may find unique applications in which their intrinsic higher energy surfaces play decisive roles.

Acknowledgment. This work was supported partly by a Grant-in-Aid for Scientific Research (A) (No. 19205030) from the Ministry of Education, Culture, Sports, Science and Technology, Japan and JST, CREST. We are grateful to Prof. Y. Katayama of Kyushu University for the use of Malvern Zetasizer Nano ZS. T.S. acknowledges the support of JSPS Research Fellowship of Young Scientists.

Supporting Information Available: TEM, SEM images, and XPS data of gold nanoplates. This material is available free of charge via the Internet at http://pubs.acs.org.

JA904910M

(41) Smoluchouwski, R. *Phys. Rev.* **1941**, *60*, 661.
(42) Barden, W. R. T.; Singh, S.; Kruse, P. *Langmuir* **2008**, *24*, 2452.
(43) Tsunoyama, H.; Ichikuni, N.; Sakurai, H.; Tsukuda, T. *J. Am. Chem. Soc.* **2009**, *131*, 7086.
(44) Yoon, B.; Häkkinen, H.; Landman, U. *J. Phys. Chem. A* **2003**, *107*, 4066.
(45) See Figure S10 in the Supporting Information.